BIOCHEMISTRY
including biophysical chemistry & molecular biology

ARTICLE

pubs.acs.org/biochemistry

Signaling Kinetics of Cyanobacterial Phytochrome Cph1, a Light Regulated Histidine Kinase

Georgios Psakis,[†] Jo Mailliet,[†] Christina Lang,[†] Lotte Teufel,[†] Lars-Oliver Essen,[‡] and Jon Hughes[*,†]

[†]Institute for Plant Physiology, Justus Liebig University, Senckenbergstrasse 3, D35390 Giessen, Germany

[‡]Department of Chemistry, Philipps University, D35032 Marburg, Germany

Supporting Information

ABSTRACT:

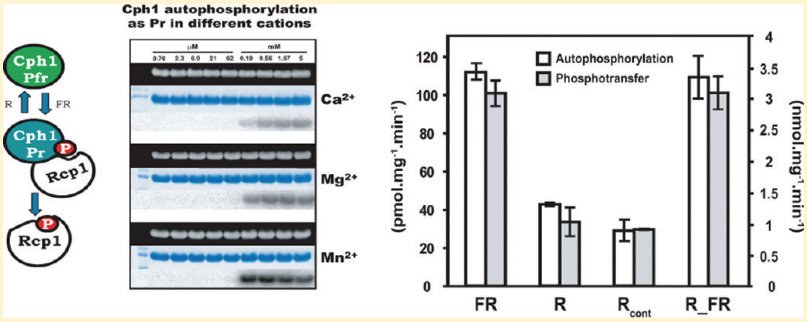

Cyanobacterial phytochrome 1 (Cph1) is a red/far-red light regulated histidine kinase, which together with its response regulator (Rcp1) forms a two-component light signaling system in *Synechocystis* 6803. In the present study we followed the *in vitro* autophosphorylation of Cph1 and the subsequent phosphotransfer to Rcp1 in different ionic milieus and following different light treatments. Both processes were red/far-red reversible with activity manifested in the Pr ground state (in darkness or after far-red irradiation) and with strongest activities being exhibited in the presence of Mn^{2+}. *In vivo* and *in vitro* assembled holoproteins in the Pr state displayed at least 4-fold higher efficiencies (k_{cat}/K_m) for autophosphorylation and phosphotransfer than the apoprotein or the holoprotein at photoequilibrium in red light. The reduced activities observed following red light treatments were consistent with the Pfr state being enzymatically inactive. Thus, both the rate of kinase autophosphorylation and the rate of phosphotransfer regulate the phosphorylation state of the response regulator, consistent with the rotary switch model regulating accessibility of the histidine target.

Perception of external cues is essential in the life of an organism as it provides the basis for acclimation to the environment. Whether a stimulus comes in the form of light, osmotic potential, temperature, oxygen, ions, or organic compounds, sensory proteins receive the signal, translate it into intramolecular chemical reactions, and pass them on to interacting proteins which finally initiate the cellular response. In microorganisms these regulatory processes are commonly represented by "two-component" signal transduction systems paradigmatically consisting of a sensory histidine protein kinase (SHPK) and a cognate response regulator. Generally, the SHPK comprises an N-terminal sensory module and a C-terminal catalytic transmitter module. In the latter, an ATP-binding domain is responsible for phosphorylating a conserved histidine residue carried on a helix−loop−helix domain. Subsequently, this phosphate is transferred to the response regulator, the second component. The *Synechocystis* 6803 genome[1] encodes at least 80 proteins involved in two-component signaling.[2] These include cyanobacterial phytochrome 1 (Cph1) and its response regulator Rcp1.[3,4]

Phytochromes are red/far-red photochromic dimeric photoreceptors ubiquitous in plants and known in many microorganisms. The N-terminal photosensory module comprising PAS (Period/Arnt/Singleminded), GAF (mammalian cGMP-binding PDEs, *Anabaena* adenylyl cyclases, and *Escherichia coli* FhlA; a structural homologue of PAS),[5] and PHY (phytochrome specific; a structural homologue of GAF)[6] domains is conserved among bacteria, fungi, and plants. In plant and various cyanobacterial phytochromes including Cph1, a linear tetrapyrole (bilin) chromophore is covalently attached to a conserved cysteine residue within the GAF domain,[6−10] whereas fungal phytochromes and bacteriophytochromes use a conserved cysteine close to the N-terminus.[11,12] Phytochromobilin (PΦB),[7,10] phycocyanobilin (PCB),[6,8,13] and biliverdin (BV)[11,12,14] are the chromophores for plant, cyanobacterial, and fungal phytochromes/bacteriophytochromes, respectively. Generally, the Pr ground state preferentially

Received: April 21, 2011
Revised: June 1, 2011
Published: June 02, 2011

dx.doi.org/10.1021/bi200612d | *Biochemistry* 2011, 50, 6178–6188

absorbs red light and is thereby photoconverted to the far-red-absorbing Pfr state. Pfr is thermally stable but can be photoconverted back to Pr in far-red light. This phototransformation is mediated by the *cis* to *trans* ($Z \rightarrow E$) isomerization of the chromophore D ring with respect to the C15=C16 double bond. Consequently, upon red light irradiation, the phytochrome switches from a *ZZZssa* configuration in Pr to a *ZZEssa* configuration in Pfr, where Z/E and s/a (*syn/anti*) respectively define the configuration of the double and single bonds at C5, C10, and C15.[6,15,16] It seems indeed that a $Z \rightarrow E$ photoflip of the D ring is the photochemical trigger in all canonical phytochromes and bacteriophytochromes.[6,14−25] Phytochrome C-termini show more or less striking similarities to SHPK transmitter modules.[26] Cph1 displays histidine autophosphorylation *in vitro* in the Pr state, following which the phosphoryl group is transferred to the acceptor Asp-68 of Rcp1.[4,8] To date and despite the substantial amount of information obtained since the discovery of Cph1, no thoroughgoing enzymatic analysis of light-regulated signaling has been published, although extensive kinetics have been performed to characterize other two-component systems. Here, we report Michaelis−Menten kinetic analyses of the autokinase and phosphotransfer activities of Cph1. We show that Mn^{2+} is the preferred cofactor for the kinase, contrary to expectations, and that both autophosphorylation and phosphotransfer transfer activities are tightly and reversibly controlled by red and far-red light, the Pfr state being enzymatically inactive. As domain-swapping experiments have shown that the intramolecular mechanism regulating transmitter activity in SHPK's is conserved, the ease and speed with which Cph1 can be (de)activated makes it a useful experimental platform for investigating the switching and phosphotransfer mechanisms at the heart of two-component signaling or for light-steered applications in synthetic biology.

EXPERIMENTAL PROCEDURES

All chemicals were purchased from Applichem (Darmstadt, Germany) unless otherwise stated.

Bacterial Strains and Gene Expression. Full length Cph1 was heterologously expressed with a C-terminally engineered hexahistidine tag in *Escherichia coli* BL21Pro cells (Clonetech).[27] For *in vivo* holophytochrome production, the bilin biosynthetic pathway was provided by plasmid p171 harboring the *pcyA* and *ho1* genes from *Synechocystis* 6803.[27,28] Rcp1 was heterologously expressed with a C-terminally engineered hexahistidine tag in *E. coli* DH5α cells (Invitrogen).[8]

Protein Purification. *In vivo* assembled Cph1 holoprotein, Cph1 apoprotein and Rcp1 were purified as previously described[8,27,29,30] with the modifications indicated in the Supporting Information. Purified apoCph1 was autoassembled with excess PCB *in vitro* in TES-β supplemented with 20% glycerol (v/v) or 20% D-xylitol (w/v). Size exclusion chromatography (SEC) on a HiLoad 16/60 or 26/60 Superdex 200 (GE Healthcare)[8] was used as the final purification step but also as a measure of the homogeneity and oligomeric state of all protein preparations. Chromatography was performed on a purpose-built ÄKTA purifier (GE Healthcare). The purity of *in vivo* and *in vitro* assembled holophytohrome was determined from their corresponding specific absorbance ratios (SAR).[8,29] R/FR difference spectroscopy was used as a relative measure of Cph1 amounts alongside Bradford assays[31] of total protein using IgG as the standard.

SDS−Polyacrylamide Gel Electrophoresis. Aliquots from autokinase and phosphotransferase reactions were terminated at specific time points as described.[4,32,33] Cph1 and Cph1/Rcp1 reaction mixtures were resolved on 12% and 15% gels, respectively, using the Laemmli buffer compositions.[34] Covalent attachment of PCB was confirmed by Zn^{2+}acetate (Merck) staining.[35]

UV−vis Spectroscopy. Absorbance spectra of holoCph1 solutions were recorded on a modified 8453 diode-array detector spectrophotometer (Agilent). To determine Pr to Pfr conversion rates, Cph1 at ca. 200 μg/mL was placed in a cuvette with polished side windows and irradiated with saturating far-red light to ensure full occupancy of the Pr state. Photoconversion to Pfr by collimated red light from a projector fitted with an interference filter (λ_{max} = 660 nm, T_{max} = 37%, fwhm = 16 nm) was monitored at 705 nm in a modified UV-mini 1240 spectrophotometer (Shimadzu). Quantum yields were determined as described[36,37] (see Supporting Information for details).

The extinction coefficient of *in vivo* assembled Cph1 as Pr at $\lambda_{max\,660}$ was determined using three separate methods, namely (1) from the absorbance of samples whose total protein concentration had been determined accurately by Bradford assay, (2) from UV−vis absorbance spectra of samples at equal concentrations in TES-β (native conditions) and 8 M urea at pH 2.0 (denaturing acidic conditions) based on the extinction coefficient at λ_{max} for denatured phycocyanin and PCB under acidic conditions (35.5 and 37 mM^{-1} cm^{-1}, respectively[38]), and (3) from absorbance spectral calibrated by the calculated extinction coefficient of holoCph1 at 280 nm.

Autophosphorylation of Cph1 Apo- and Holophytochromes. Purified Cph1 (10 μM) was phosphorylated in 50 mM Tris-HCl, 150 mM NaCl, 50 mM KCl, 10% glycerol (v/v), 1 mM DTT, 5 mM $MgCl_2$, pH 7.8 supplemented with 1 mM ATP containing 0.01% [γ-^{32}P] ATP (222 TBq, $mmol^{-1}$, Perkin-Elmer), as previously described.[4,33,39] Terminated reactions were analyzed by SDS-PAGE. The dye front was removed to reduce background radiation from unincorporated ^{32}P. Dried gels were placed on a phosphor-image screen for 16−18 h. For direct comparisons of the tested conditions, exposure times were kept constant and when possible the gels to be compared were exposed on the same screen. The images were read out using a Fuji FLA-7000 phosphor-imager and signals quantified by signal intensity (photostimulated luminescence: PSL units) against known standards, using the AIDA Image Analyzer 4.22 software. Background counts were measured for every lane and were subtracted from the corresponding signals.

All optimizations were performed on *in vivo* holo-Cph1 in the Pr state. For determination of the preferred by Cph1 divalent cation, $MgCl_2$ was replaced by the same concentration of $CaCl_2$, $CoCl_2$ (Sigma), $MnCl_2$ (Sigma), $NiCl_2$, $RbCl_2$ (Aldrich), $SnCl_2$ (Merck), or $ZnCl_2$ (Merck), and kinase activities were studied for both Pr and Pfr/Pr states. These experiments were also conducted in the presence of 1 mM EDTA or 1 mM EGTA. In the latter case three master mixes were prepared: one containing protein and buffer, one containing the source of cation and ATP, and one containing the chelating agent. Reactions were initiated with the concomitant addition of cation/ATP and chelator to the phytochrome master mix and followed for an hour at 25 °C. Test phosphorylations were also carried out using 760 nM to 5 mM $CaCl_2$, $MgCl_2$, or $MnCl_2$. To identify any synergistic effects of these ions on the protein's kinase activity, combinations of $CaCl_2$/$MgCl_2$, $CaCl_2$/$MnCl_2$, $MgCl_2$/$MnCl_2$, and $CaCl_2$/$MgCl_2$/$MnCl_2$ were tested at 62−190 μM concentrations. Finally, the optimum pH of autokinase activity was determined from a tested 6.8−9.3 range. Initial autophosphorylation rates were determined for each ATP concentration (5 μM to 1 mM) and for every phytochrome preparation (in Pr or Pfr/Pr) from early points of the linear phase of the reaction (2−10 min). Experiments were carried out in triplicate. Kinetic parameters were calculated from the least-squares fit to Michaelis−Menten hyperbolae and qualitatively compared to those derived from Hanes−Wolf linearizations (GraphPad Prism; Cambridge Scientific).

Phosphotransfer of Phosphorylated Cph1 Apo- and Holophytochromes to Rcp1. Following Cph1 (23 μM) autophosphorylation (100 mM ATP for 1 h, as Pr or in Pr/Pfr photoequilibrium mixture), ATP was removed from the mixture by gel filtration (Illustra MicroSpin NAP-25 columns; GE Healthcare) and 10 μM protein mixed with Rcp1 (0.2−33 μM in phosphorylation buffer without ATP) for initiation of the transfer reaction. Reactions were terminated as above. The rate of phosphotransfer from Cph1 was determined from early points of the linear phase of the decay (up to 2 min). Assays were performed in triplicate.

Light Treatments. Autokinase and phosphotransfer assays were also conducted under conditions of continuous and pulsed irradiations, in particular to ascertain the activities of Pfr. For autophosphorylation experiments, *in vivo* assembled Cph1 holophytochrome in its Pr state at 10 μM was irradiated with either continuous red light (λ_{max} = 660 nm, fluence rate = 6.7 μmol m^{-2} s^{-1}; R), or with 1 min pulse of saturating (1) R, (2) far red (λ_{max} = 730 nm, fluence rate = 2.3 μmol m^{-2} s^{-1}; FR), (3) R_FR, (4) R_FR_R, (5) FR_R, and (6) FR_R_FR light prior to the initiation of the reaction. For the continuous R condition, the reaction was initiated by adding the appropriate divalent ion/ATP concentration after a 1 min preirradiation in R. Reactions were allowed to proceed for 2−10 min before termination.

The same methodology was followed to investigate the effect of light on the phosphotransfer reaction itself. *In vivo* assembled Pr holophytochrome (23 μM) was phosphorylated (100 μM ATP) at 25 °C, for 1 h in darkness, ATP subsequently removed by gel filtration, and the mixture subjected to either continuous R or 1 min pulse of saturating (1) R, (2) FR, and (3) R_FR light treatments before mixing Cph1 (10 μM end concentration) with excess Rcp1. Reactions were allowed to proceed for 2 min.

RESULTS

Photochemical Parameters and Sample Purity. The extinction coefficient of *in vivo* assembled holoCph1 in its Pr state ($\lambda_{max,red}$ = 661 nm) was determined by three different methods. A value of 89.1 ± 2.5 mM^{-1} cm^{-1} was derived from the extinction coefficient of phycocyanin in acid urea.[38] Direct measurements required the concentration of Cph1 to be known exactly (despite traces of impurities). The protein concentration of highly purified samples was derived from IgG-calibrated Bradford assays, yielding an extinction coefficient at 661 nm of 88.3 ± 1.2 mM^{-1} cm^{-1}. As an alternative, $\varepsilon_{280\,nm}$ of native full length Cph1 was derived based on the assumption that ε_{280} of urea-denatured Cph1 is identical to the value calculated from the protein sequence plus that of the chromophore in neutral urea buffer. The theoretical $\varepsilon_{280\,nm}$ of the recombinant apoCph1 (85 mM^{-1} cm^{-1}; Vector NTI, Invitrogen) with a contribution of 3.8 ± 0.3 mM^{-1} cm^{-1} from PCB in urea,[8] resulted in a value of

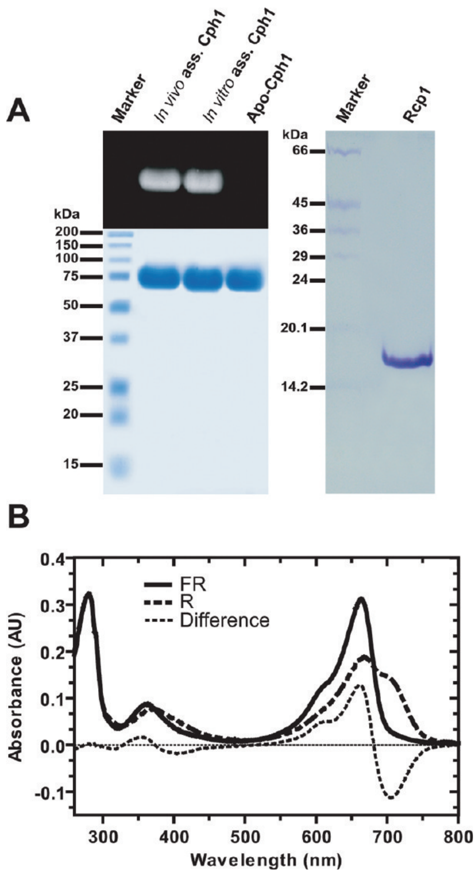

Figure 1. SDS-PAGE and UV−vis absorbance spectra of *in vivo* and *in vitro* assembled Cph1 holoproteins and Rcp1. (A) SDS-PAGE of purified holo-Cph1 (*in vivo* and *in vitro* assembled), apo-Cph1 (left) and Rcp1 (right). Covalent PCB assembly was confirmed by zinc acetate staining (upper left). (B) UV−vis absorbance spectra of purified *in vivo* assembled Cph1 in TES-β after far-red (FR) and red irradiation (R). The difference spectrum is also shown.

88.5 mM^{-1} cm^{-1} for holoCph1 which could be used to calibrate the UV−vis absorbance spectrum of highly purified material. As the 280 and 661 nm peaks were equal, the 661 nm extinction coefficient was thereby also 88.5 mM^{-1} cm^{-1} for holoCph1. On the basis of the maximal 661 nm:280 nm specific absorbance ratio (SAR) of 1.0 corresponding to 100% purity, *in vivo* and *in vitro* assembled holoproteins routinely used here were purified to more than 96% (Figure 1A,B) and 85% homogeneity respectively (Figure 1A). The purity of Rcp1 was more than 95% as judged by SDS-PAGE (Figure 1A).

Initially, we followed photoconversion from Pr to Pfr for 5 min (Figure S1A,B) in phosphorylation buffer without divalent cations [50 mM Tris-HCl, 150 mM NaCl, 50 mM KCl, 10% glycerol (v/v), 1 mM DTT, pH 8.1, 1 mM ATP]. Both *in vivo* and *in vitro* assembled holoproteins displayed the same photochemical behavior. The rate constants for their phototransformation using 660 nm actinic light (8.1 μmol m^{-2} s^{-1}), and monitoring absorbance at 705 nm, were almost identical (0.0122 ± 0.0004 and 0.0130 ± 0.0001 s^{-1}, respectively; Figure S1A,B). $X_{Pfr,max}$, the Pfr molar occupancy in red light, was determined as 0.70 for the Cph1 sensory domain for which pure Pfr can be obtained by SEC.[40] Using this value for the full length holoprotein assembled *in vivo* and *in vitro* yielded hypothetical Pfr spectra identical to those measured for the purified Pfr dimer of the sensory domain;

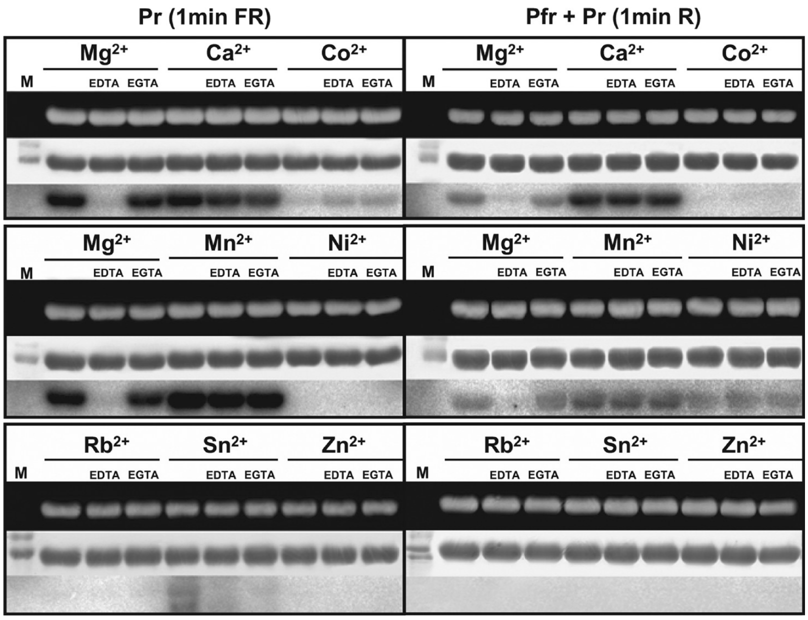

Figure 2. Autophosphorylation of *in vivo* assembled Cph1 following far-red (FR) and red (R) irradiations in the presence of Mg^{2+}, Ca^{2+}, Co^{2+}, Mn^{2+}, Ni^{2+}, Rb^{2+}, Sn^{2+}, and Zn^{2+} ions at 5 mM. Each block describes the effects of three ions on the autokinase activity. In each block the top, middle, and bottom rows correspond to zinc acetate fluorescence, Coomassie staining, and phosphorimage of a 12% SDS-PAGE gel. The three lanes from left to right correspond to the autokinase activity in the absence of chelator and in the presence of EDTA or EGTA at 1 mM, respectively. Reactions were allowed to proceed in darkness for 1 h at 25 °C. M: molecular weight marker.

thus, $X_{Pfr,max}$ is likely to be close to 0.70 in both cases. Using the determined rates, the actinic light intensity (I_{660}), the extinction coefficients $\varepsilon_{660\ nm}$, and $X_{Pfr,max}$ 0.70 the quantum yields [$\Phi_r = (k_{660}[Pfr]_{\infty}^{660})/(I_{660}\varepsilon_{r660})$][41] of the Pr to Pfr phototransformation for the *in vivo* and *in vitro* assembled Cph1 were 0.118 ± 0.004 and 0.132 ± 0.001, respectively. Pr to Pfr photoconversion rates for *in vivo* assembled Cph1 in the presence of 5 mM Mg^{2+}, Mn^{2+}, and Ca^{2+} were also measured. Mg^{2+} or Mn^{2+} had insignificant effects (Figure S1A,B). With 5 mM Ca^{2+}, however, $A_{660\ nm}$ values fell slowly in darkness (Figure S1C) accompanied by increasing scattering apparent from increasing OD toward shorter wavelengths, implying aggregation. Consequently, the maximal absorbance at 705 nm in the presence of Ca^{2+} (Figure S1A,D) was lower than the controls ± Mg^{2+} or Mn^{2+}. For Ca^{2+}, the photoconversion rate and phototransformation yield were 0.0094 ± 0.0001 s^{-1} and 0.091 ± 0.001, respectively.

Optimization of Cph1 Autophosphorylation. *In vivo* assembled Cph1 holoprotein mediates its own ATP-dependent phosphorylation in the Pr state.[4] The dependence of autokinase activity on the type of divalent ion available was investigated initially using 5 mM divalent ions.[42] Surprisingly, Mn^{2+} resulted in higher activities than other divalent cations (Figure 2). Following red irradiation, the Pfr/Pr photoequilibrium mixture displayed a dramatic reduction in autophosphorylation in the presence of Mg^{2+} consistent with previous reports.[4] This was also seen for Mn^{2+} whereas Ca^{2+} resulted in ca. 50% reduced activity of the Pr/Pfr mixture relative to 100% Pr (Figure 2). 5 mM Ni^{2+}, Rb^{2+}, Sn^{2+}, or Zn^{2+} precipitated the protein and did not support autophosphorylation.

The effects of chelators on Pr autokinase activity were studied (Figure 2). With 5 mM Mn^{2+}or Ca^{2+} 1 mM EDTA caused a 1.5-fold reduction of the observed signal, whereas, consistently, the same test with Mg^{2+} largely abolished the kinase activity. Addition of 1 mM EGTA halved the kinase activity in Mg^{2+} or Ca^{2+}, but was less effective with Mn^{2+} (Figure 2). Basal kinase activity was displayed in the presence of Co^{2+} and was mildly increased after the addition of chelator (Figure 2).

To define the range of optimal ion concentration for autokinase activity, we lowered the initial 5 mM concentration in increments of three to 760 nM. In agreement with the data above the following preference was indicated: $Mn^{2+} > Mg^{2+} > Ca^{2+}$ (Figure 3A). Activity was barely detectable for all tested ions at 62 μM and was undetectable for lower concentrations (Figure 3A). A sharp increase in activity was observed for Mn^{2+} and Mg^{2+} at 190 μM, which peaked at 560 μM, higher concentrations appearing inhibitory (Figure 3A,B). Increased Ca^{2+} resulted in a continuous increase, however (Figure 3B). Combinations of Mn^{2+}/Ca^{2+} or Mn^{2+}/Mg^{2+} resulted in slightly higher activities than those displayed in Ca^{2+} or Mg^{2+} alone but never equaled that in Mn^{2+} (Figure S2). The Ca^{2+}/Mg^{2+} combination resulted in higher activities than those shown in Ca^{2+} alone, but Mg^{2+} alone was still more effective. With Mn^{2+}, Ca^{2+}, and Mn^{2+} present at equal concentrations (total concentration 190 μM), the activity was significantly lower than that for Mg^{2+} or Mn^{2+} at 190 μM. With the optimal divalent ion concentration determined (560 μM Mn^{2+}) we proceeded with the determination of the optimum pH for autokinase activity. Tris-HCl was used to achieve an overall pH in solution from 7 to 9. An optimum pH of 8.15−8.20 was observed (Figure S3C).

Michaelis−Menten Kinetics for Cph1 Autophosphorylation. Reactions were linear for the first 20 min and reached a plateau over a period of 2 h (Figure S3A,B). Autophosphorylation rates were determined from the linear phase of the reactions and plotted against [ATP]. Autokinase rates showed the anticipated Michaelis−Menten behavior with respect to [ATP] (Figure 4A). *In vivo* and *in vitro* assembled holoproteins in Pr showed similar K_m values for autophosphorylation (7−11 μM, Table 1; $P = 0.17$). V_{max} values were 133 and 154 pmol mg^{-1} min^{-1}

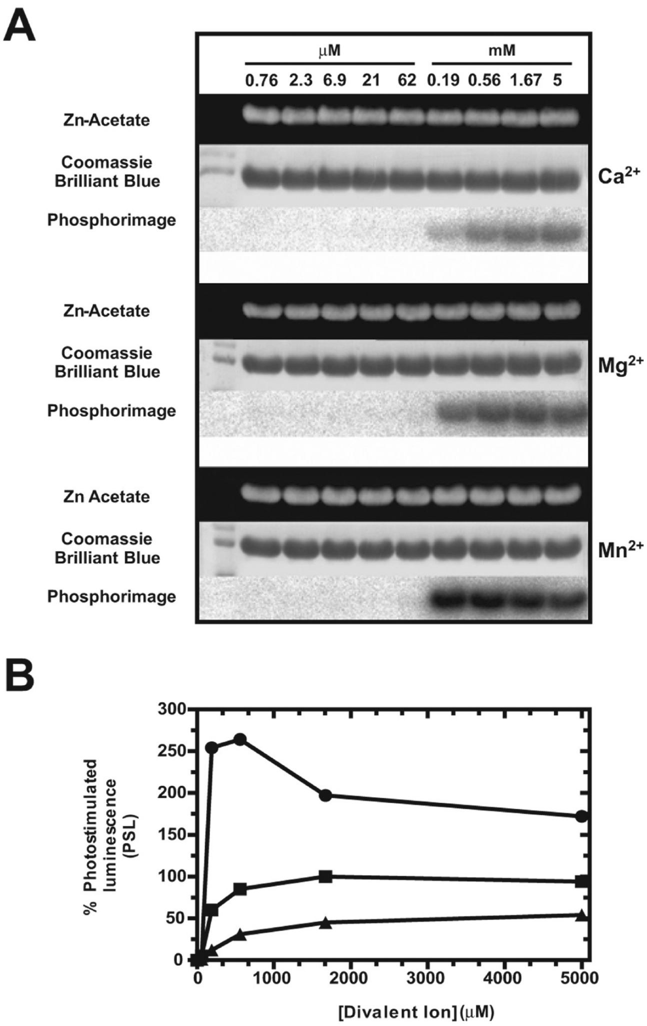

Figure 3. Dependence of *in vivo* assembled Cph1 autokinase activity as Pr on Ca^{2+}, Mg^{2+}, and Mn^{2+} concentrations. (A) Images (blocks as in Figure 2) and (B) quantified phosphoimage signals for Ca^{2+} (triangles), Mg^{2+} (squares), and Mn^{2+} (circles). Reactions were allowed to proceed in darkness for 1 h at 25 °C.

respectively corresponding k_{cat} and k_{cat}/K_m values (Table 1), suggesting similar turnovers and enzymatic efficiency. The V_{max} values for the autophosphorylation of the *in vivo* and *in vitro* Pfr/Pr mixes were 4-fold and 6-fold lower than those of their Pr counterparts, whereas the K_m values remained unchanged. *In vivo* and *in vitro* holoprotein Pfr/Pr mixes showed 9-fold and 3-fold lower k_{cat}/K_m than that observed for their corresponding Pr states.

Although the V_{max} for the autokinase activity of the apoprotein was only slightly greater than that of the Pr holoprotein, the K_m was more than 20-fold higher, making it a less efficient enzyme (k_{cat}/K_m = 2 M^{-1} s^{-1}) than Pr. There was, overall, good agreement between the parameters derived from the hyperbolic fits and from linear transformations (Table S1).

Rcp1-P Formation and Kinetics of Phosphotransfer. Tests of autophosphorylations (10 μM *in vivo* assembled Cph1) with varying concentrations of $MnCl_2$ or $MgCl_2$ (21 μM to 5 mM) and subsequent phosphotransfer assays (33 μM Rcp1) were conducted for 1 h at 25 °C in the presence of ATP. Reactions were terminated by addition of stop buffer and analyzed as before. As for the autokinase, the coupled kinase/phosphotransferase activity was significantly higher with Mn^{2+} than with the other tested cations (Figure S4). Although Mn^{2+} or Mg^{2+} at the 560 μM optimum for autophosphorylation supported efficient phosphotransfer to Rcp1, the optimum in the latter case was closer to 1.7 mM (Figure S4).

The phosphotransfer reaction itself was investigated by first phosphorylating Cph1 alone, removing the unused ATP and only then adding Rcp1. Phosphorylated Cph1 as Pr was dephosphorylated in the presence of Rcp1 (Figure 5A), in accordance with previous observations.[4,8] Cph1 autophosphorylation following red irradiation (Pfr/Pr mix) was lower with the expected effect on Rcp1 phosphorylation. The Rcp1-dependent dephosphorylation of Cph1 followed a hyperbolic time course with a linear phase within the first 2 min of the reaction and plateaued over a period of 1 h (Figure 5B). In the absence of Rcp1, the phosphorylated Cph1 was quite stable showing a half-life of about 50 min, whereas the half-life of phosphorylated Rcp1 was ~2 min (Figure 5C). The kinetic properties of the phosphotransfer reaction from Pr to Rcp1 were very different (Figure 4B): V_{max} was ~30-fold higher and K_m about half that for autophosphorylation. Light effects on the two reactions, however, were very similar (Table 1). Phosphotransfer rates for in *vivo* and *in vitro* reconstituted holoproteins in the Pr state were 4–6-fold faster than their counterparts in the Pfr/Pr mixture and for the apoprotein (Figure 4B). There was again reasonable agreement between the parameters derived from the hyperbolic fits and from Hanes–Wolf linearizations.

Light Control of the Autokinase Activity and Phosphotransfer Capability of Cph1. Treatment of the holoprotein with 1 min red light (R) caused a ~ 62% reduction in autokinase activity, in line with expectations. Under conditions of continuous red light (Figure 6A), a ~10% further reduction in activity was observed. R_FR and FR_R_FR treatments restored the maximum activity observed for FR irradiated (Pr) samples (Figure 6A), whereas the R_FR_R and FR_R pulse sequence again resulted in a 2–3-fold reduction of the autokinase activity.

To study photoreversibility of phosphotransfer independently of Cph1 autophosphorylation, *in vivo* assembled holoprotein samples were phosphorylated following the previous light treatments, ATP removed, and Rcp1 added (Figure 6B). Dark and FR-treated samples behaved similarly and displayed the highest activities. There was a 3-fold reduction in the phosphotransfer rate following the R pulse treatment and a further small reduction under continuous R, closely reflecting the effects on autokinase activity described above. Similarly, pulse sequences ending with FR restored the higher phosphotransfer rates of the FR treated sample, whereas those ending with R resulted in ~2-fold lower activities (Figure 6B). The same trends emerged when *in vivo* assembled holoprotein was phosphorylated in darkness and then subjected to R, R_{cont}, and R_FR treatments before initiation of the phosphotransfer reactions by addition of Rcp1 (Figure 6C).

■ DISCUSSION

To date, the photochemical parameters of Cph1 (and indeed other phytochromes) have been assumed to be identical for apoprotein assembled with excess chromophore *in vitro* and material probably cotranslationally assembled *in vivo*. From the mean of three independent methods, we estimate the extinction coefficient of holoCph1 generated *in vivo* to be 88.6 mM^{-1} cm^{-1}, closely similar to that of *in vitro* assembled material.[8] The rates of their Pr to Pfr photoconversion were also very similar (k_{660} =

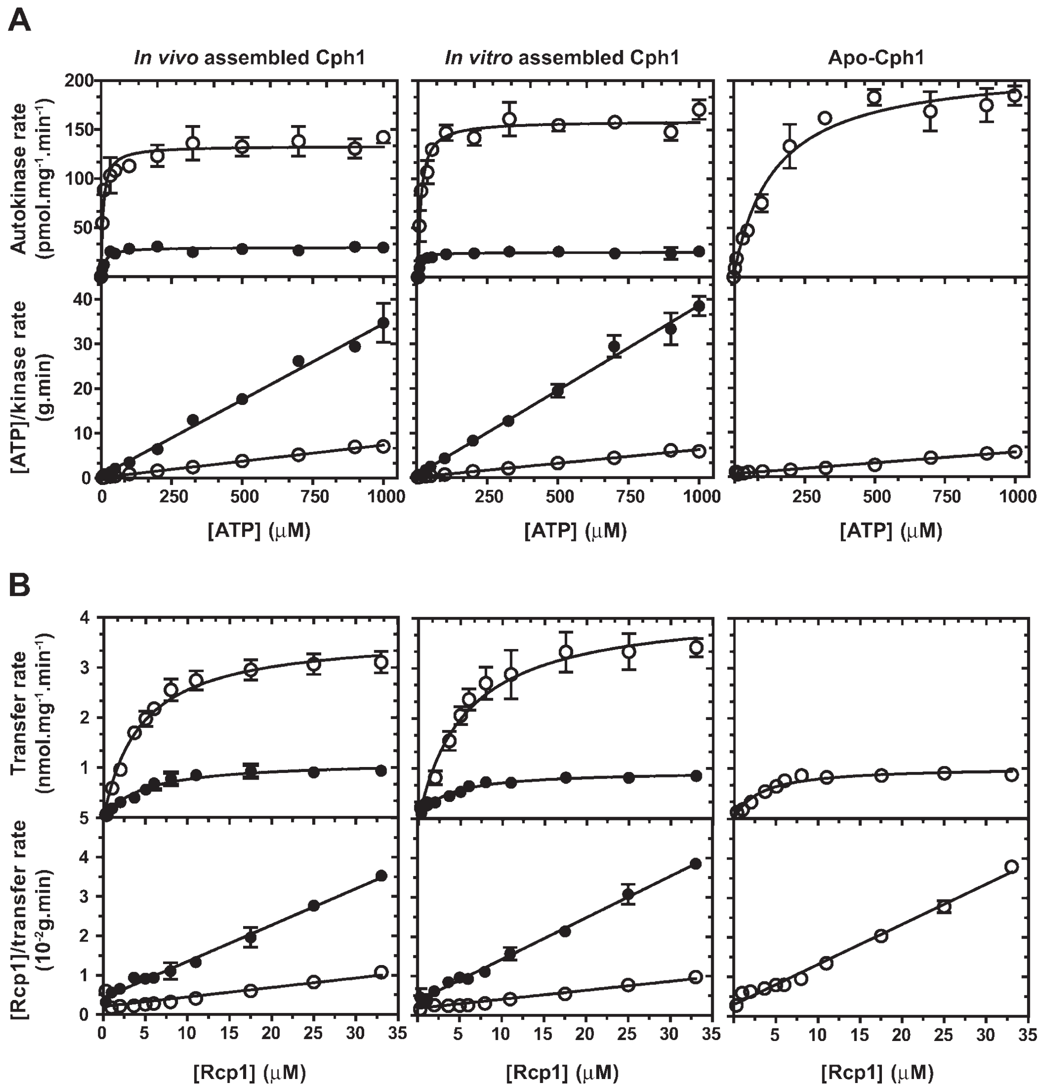

Figure 4. Michaelis–Menten kinetics of holo- and apo-Cph1 autophosphorylation and phosphotransfer to Rcp1. (A) ATP dependence of initial autophosphorylation velocities for *in vivo*- and *in vitro*-assembled holoCph1 and apoCph1 (in the absence of Rcp1). Autokinase activities of Pr and the Pr-Pfr photoequilibrium mixture are shown as open and closed circles, respectively. Above, phosphorimager data with hypobolic fits; below, linear Hanes–Wolf transformations. (B) Rcp1 dependence of initial phosphotransfer velocities for holo- and apo-Cph1 after removal of ATP. Symbols as in (A). The bars in each panel show the standard error of triplicate measurements.

0.012–0.013 s^{-1}) regardless of the presence or absence of ions in the tested buffer. Subtraction of 30% of the Pr absorbance spectrum from the absorbance spectrum at photoequilibrium in red light resulted in a hypothetical 100% Pfr spectrum which closely matched that of the Cph1 sensory module purified to 100% Pfr occupancy by SEC.[40] Thus, the Pfr mole fraction at photoequilibrium in red light ($X_{\mathrm{Pfr,max}}$) for full length Cph1 as well as the separate photosensor module assembled either *in vivo* or *in vitro* is ~0.70. As the extinction coefficients, phototransformation rates and photoequilibria were similar, so were the quantum yields of photoconversion (Φ_r = 0.12–0.13).

The work reported here describes the effects of divalent ions, pH, and light on the regulation of the autokinase activity of Cph1 and the subsequent control of phosphotransfer to the cognate response regulator Rcp1. In agreement with previous reports,[4,8] Cph1 Pr is the active histidine kinase, capable of autophosphorylation and subsequent transfer of the phosphate to the aspartyl-Rcp1. Whether the Pfr state is fully inactive is hard to determine because—in contrast to the free sensory module[40]—it cannot be produced at 100% occupancy (i.e., free of Pr). Nevertheless, the 70/30 Pfr/Pr photoequilibrium mixture displays a 62–74% lower kinase activity relative to that of Pr, consistent with complete inactivity of Pfr and $X_{\mathrm{Pfr,max}}$ of 0.70. Similarly, the subsequent transfer of the labeled phosphate from phosphorylated Cph1 to Rcp1 is consistent with Pfr being inactive. These results are in qualitative agreement with previous reports[4] in which, however, a $X_{\mathrm{Pfr,max}}$ value of 0.87 (based on plant phytochrome data) was assumed. Accepting the $X_{\mathrm{Pfr,max}}$ value of 0.70 for Cph1, all data are consistent with this state being inactive both as an autokinase and as a phosphotransferase. Although a true negative control in which Pr is absent is not available in the case of Cph1, in "bathy" phytochromes like PaBphP Pfr is the ground state. Extrapolating from Cph1, this would be enzymatically inactive in contrast to an active Pr. Interestingly, PaBphP autokinase activity was reported to show only weak state dependency, however.[43]

dx.doi.org/10.1021/bi200612d |*Biochemistry* 2011, 50, 6178–6188

Table 1. Michaelis–Menten Parameters of Autokinase and Phosphotransfer Activities of Holo- and Apo-Cph1

	autokinase			
protein	K_m (μM)	V_{max} (pmol/(mg min))	k_{cat} (10^{-4} s^{-1})	k_{cat}/K_m (M^{-1} s^{-1})
*in vivo*_Pr	7 ± 2	133 ± 4	2.0 ± 0.1	28 ± 8
*in vivo*_Pfr/Pr	12 ± 2	30 ± 1	0.40 ± 0.03	3 ± 1
*in vitro*_Pr	11 ± 2	154 ± 4	2.2 ± 0.1	20 ± 4
*in vitro*_Pfr/Pr	7 ± 2	25 ± 1	0.41 ± 0.02	6 ± 1
Apo	144 ± 23	216 ± 10	3.0 ± 0.1	2 ± 0.4
	phosphotransfer			
protein	K_m (μM)	V_{max} (pmol/(mg min))	k_{cat} (10^{-4} s^{-1})	k_{cat}/K_m (M^{-1} s^{-1})
*in vivo*_Pr	4 ± 1	3672 ± 146	51 ± 2	1159 ± 164
*in vivo*_Pfr/Pr	5 ± 1	1129 ± 72	16 ± 1	340 ± 69
*in vitro*_Pr	6 ± 1	4225 ± 292	59 ± 4	1054 ± 255
*in vitro*_Pfr/Pr	3 ± 1	953 ± 45	14 ± 1	467 ± 159
Apo	3 ± 1	1033 ± 42	14 ± 1	467 ± 159

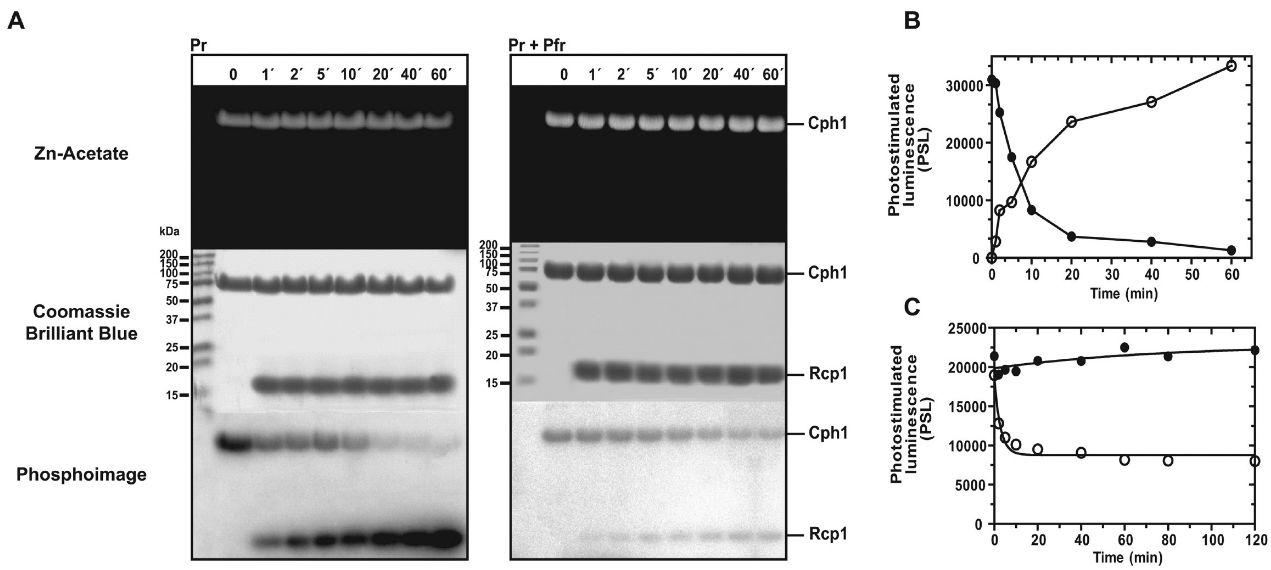

Figure 5. Phosphotransfer activity of *in vivo* assembled Cph1 to Rcp1 (at 10 and 33 μM, respectively). (A) Phosphotransfer activities of Cph1 in the presence of ATP. Cph1 samples were phosphorylated following 1 min far-red (Pr) or 1 min red (Pfr/Pr mix) irradiation by addition of 100 μM ATP. Phosphotransfer reactions were performed for 1 h in darkness at 25 °C. (B) Cph1 (closed circles) and Rcp1 (open circles) phosphorylation kinetics. (C) Stability of Cph1 (closed circles) and Rcp1 (open circles) phosphorylated species following ATP removal.

Earlier work on Cph1[4] reported autophosphorylation in the presence of 5 mM Mg^{2+}.[4,42] Similarly, autophosphorylation of *PaBphP* and *Agrobacterium tumerfaciens* Agp1 was described in 5 mM $MgCl_2$,[44,45] while equivalent work on CphA and CphB from *Calothrix* sp. (*Fremyella diplosiphon*)[46] was described in the presence of 0.5 mM Mg^{2+}. We were thus surprised to find that Mn^{2+} was the divalent ion preferred by Cph1 (Figures 2 and 3A). In fact, this is not uncommon among SHPKs, suggesting that the cation preferences of other phytochromes should be verified experimentally. All of the tested Mn^{2+} concentrations resulted in 2-fold higher phosphorylation intensity for Cph1 in Pr relative to the Mg^{2+} or Ca^{2+} optima (Figures 3A). No synergism was observed between cations (Figure S2) consistent with competition for a single binding site within the ATPase domain of the histidine kinase and the affinity of the catalytic site for Mn^{2+} being higher than that for Mg^{2+} and Ca^{2+}. The optimal Mn^{2+} concentration for autokinase activity was 190–560 μM (Figure 3A), 5 mM $MnCl_2$ resulting in a marked reduction in the signal intensity implying partial poisoning. Even at optimal concentrations, Mg^{2+} lead to lower activities than for Mn^{2+}, while Ca^{2+} and especially Ni^{2+}, Rb^{2+}, Sn^{2+}, and Zn^{2+} resulted in protein precipitation. The sudden increase in autophosphorylation between 60 and 200 μM for all cations (Figure 3A) implies cooperative binding. Similarly, phosphotransfer to the Rcp1 response regulator was most efficient in the presence of Mn^{2+} (Figure S4). Interestingly, crystal structures of Rcp1[47] and of the sporulation response regulator Spo0F from *B. subtilis*[48] have been described with bound Mn^{2+}, whereas NMR studies indicate that Ca^{2+} as well as Mg^{2+} and Mn^{2+} bind to the conserved aspartate of the Spo0F regulator.[49] On the other hand, only Mg^{2+} was shown

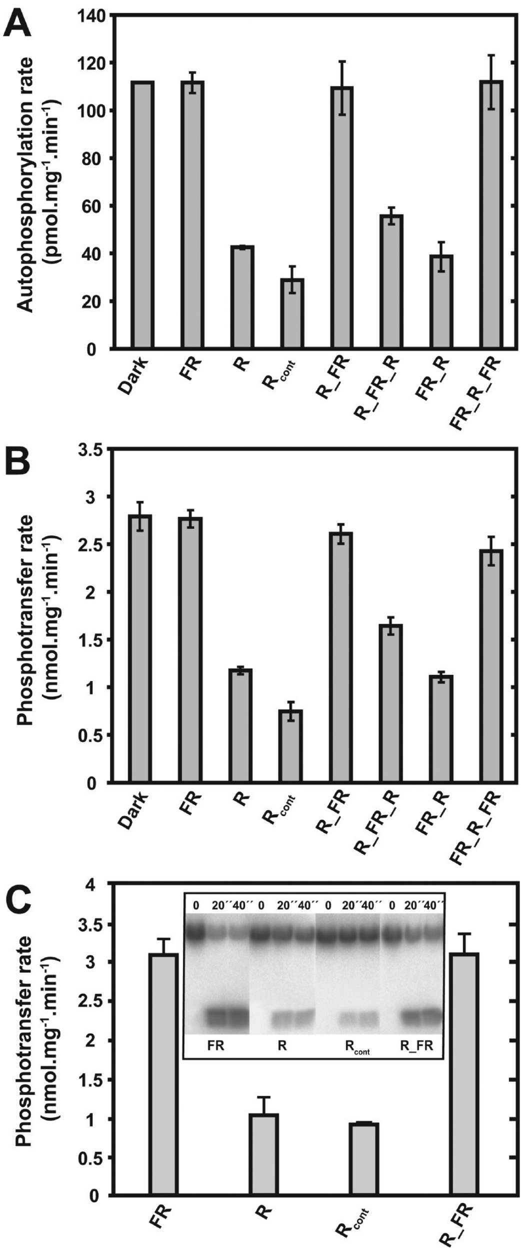

Figure 6. Light control of autokinase and phosphotransferase activities (*in vivo* assembled Cph1 and Rcp1 at 10 and 25 μM, respectively). (A) Initial rates of autophosphorylation in the presence of ATP with different light treatments [1 min FR (far red) and R (red) pulses as shown]. Protein samples were irradiated before the reaction was initiated by the addition of ions and ATP. In R_{cont} (continuous red irradiation) the sample was preincubated with red light for 1 min before the reaction was started. Phosphorylation reactions following the light treatments was allowed to proceed for 1 h at 25 °C in darkness (B) Initial phosphotransfer rates to Rcp1 following light treatments and Cph1 autophosphorylation as in (A) but with removal of unused ATP. The bars in both panels correspond to standard errors of triplicate measurements. (C) Initial phosphotransfer rates to Rcp1 following Cph1 autophosphorylation in darkness, ATP removal, and subsequent irradiation (light treatments as in (A)). Phosphotransfer reactions were initiated by addition of Rcp1 and aliquots from the phosphotransfer mix were removed after 20 and 40 s. Inset shows the corresponding phosphoimage signals—Cph1 (top) and Rcp1 (bottom)—in accordance with Figure 5. The bars in all panels correspond to standard errors of triplicate measurements.

to support phosphotransfer from KinA.[50] Although Mn^{2+} and Mg^{2+} have similar van der Waals radii (0.83 Å), Mn^{2+} is a more effective Lewis acid and a better electrostatic stabilizer.[51] It is these properties together with its tendency to bind nitrogenated groups that may possibly result in the formation of more stable kinase-cofactor complexes than Mg^{2+} or Ca^{2+}. Whether Mn^{2+} is the ion used in the native protein in *Synechocystis* is not known.

Hyperbolic fits to the Michaelis−Menten kinetics of autophosphorylation showed similar K_m values (7−11 μM, $P = 0.17$) for both *in vivo* and *in vitro* assembled Cph1 in Pr. Following red light irradiation, *in vivo* and *in vitro* Pr/Pfr mixtures showed 4- and 6-fold lower V_{max} values than their Pr counterparts, respectively, while the K_m values were unchanged (7−12 μM, $P = 0.1$). The 4-fold lower activity of the *in vivo* Pr/Pfr mix following red irradiation is consistent with $X_{Pfr,max}$ value of 0.70. The kinetics of phosphotransfer reflected generally those of autophosphorylation. The essential difference being that phosphotransfer is much faster than autophosphorylation (V_{max} ∼30-fold higher). The fact that the apoprotein itself displayed both autokinase and phosphotransfer activities would allow it a role in signaling.

Phosphorylated Cph1 was stable with a half-life of ∼50 min, whereas phosphorylated Rcp1 showed a half-life of 2 min (Figure 5C). Much longer lifetimes were reported for the RcpA and RcpB response regulators corresponding to CphA and B from *Calothrix* (*Fremyella diplosiphon*).[52] Indeed, half-lives of phosphorylated response regulators range from second to hours.[53] The half-lives of CheY and of Spo0F, for example, are ca. 0.5 min and 3 h, respectively,[54,55] in harmony with the processes controlled, namely chemotaxis and sporulation. Because of the very short half-life of phosphorylated Rcp1, we did not attempt to measure the transmitter phosphatase activity of Cph1. Interestingly, however, Cph1 lacks the conserved glutamine/asparagines of the DxxxQ or E/DxxT/N/Q motifs, shown to be essential for transmitter phosphatase activity in NarX.[56] The motifs are also present in DesK, EnvZ, and FixL for which strong transmitter phosphatase activities have been described.[57−59]

Proteolytic degradation of purified phytochrome or phytochrome-like proteins has been described.[8,33] In the case of the current Cph1 purifications, however, we did not detect any degradation for up to 4 months at 4 °C even in the absence of chelators.

Both autokinase and phosphotransfer activities are under the control of light (Figure 6). The $X_{Pfr,max}$ value of 0.70 together with the autokinase and phosphotransfer activities implies that Pfr is enzymatically inactive, consistent with earlier data.[4] Light pulse experiments showed clear R/FR photoreversibility following the classical pattern,[60] except that Pr rather than Pfr is the enzymatically active state.

The question naturally arises as to the mechanism of catalytic regulation, given that there is no evidence for a direct interaction between N-terminal sensory modules and C-terminal ATPase domains. The link between the photosensory and transmitter modules of Cph1 is provided by the α15 helix, which probably extends through the His538 phosphoacceptor. Rotation of this helix in the phytochrome dimer might change the accessibility of His538 both for the flexibly attached ATPase domain and the response regulator, a regulatory mechanism similar to that suggested for blue light regulated SHPK's.[59,61] Indeed, the 3D structure of the Cph1 sensory module[6] shows the tongue-like structure poised to register light-induced changes in the GAF domain and to transmit them to α15.

The results described in this work provide an *in vitro* template for studying signaling in Cph1 and its derivatives including site-directed mutants designed to probe the role of individual residues. Hybrid molecules like the "Cph8" chimera in which the photosensory module of Cph1 is fused to the catalytic transmitter domain of EnvZ[62] provide an alternative *in vivo* route to the same end using similar site-directed mutants. Here the light signal can drive OmpC-dependent expression of *lacZ* in *E. coli* via the EnvZ−OmpR interaction, and the resulting β-galactosidase activity can be directly assayed. Data derived from the two methods recently identified R254 and R472 as components of the signal chain.[16] Varying the length of the α15 helix of the constructed chimaeras could also prove useful for unveiling its role in intramolecular signaling. Similar methodologies have proven successful in defining the role of the Jα helix in YtvA-FixL chimaeras.[59]

ASSOCIATED CONTENT

S Supporting Information. (1) Additional details on experimental procedures (protein purifications, irradiation of purified Cph1 holophytochromes, determination of quantum yields, and determination of the half-lives of phosphoproteins); (2) a brief discussion; (3) one table of kinetic parameters; and (4) four figures. This material is available free of charge via the Internet at http://pubs.acs.org.

AUTHOR INFORMATION

Corresponding Author

*Tel: +49-641-99-35430. Fax: +49-641-99-35429. E-mail: jon.hughes@uni-giessen.de.

Funding Sources

This work was supported in part by DFG grants HU702/6 and ES152/6 and Volkswagen-Stiftung grant I/79979.

ACKNOWLEDGMENT

We thank Penelope Higgs and Andreas Schramm for useful discussions regarding the kinase and transfer assays. We are also indebted to Rupert Schmidt and David Hinchliffe for technical advice and support. We are grateful to the Deutsche Forschungsgemeinschaft (DFG) and the Volkswagen Stiftung for funding this work.

ABBREVIATIONS

Cph1, cyanobacterial phytochrome 1; Rcp1, response regulator of cyanobacterial phytochrome 1; Pr, red light absorbing form; Pfr, far-red light absorbing form; SHPK, sensory histidine protein kinase; PAS, Period/Arnt/Singleminded; fwhm, full width half-maximum; GAF, mammalian cGMP-binding PDEs, *Anabaena* Adenylyl cyclases, and *Escherichia coli* FhlA; PDE, phosphodiesterase; PHY, phytochrome; PΦB, phytochromobilin; PCB, phycocyanobilin; BV, biliverdin; SEC, size exclusion chromatography; SAR, specific absorbance ratio; R, red light; FR, far-red light.

REFERENCES

(1) Kaneko, T., Sato, S., Kotani, H., Tanaka, A., Asamizu, E., Nakamura, Y., Miyajima, N., Hirosawa, M., Sugiura, M., Sasamoto, S., Kimura, T., Hosouchi, T., Matsuno, A., Muraki, A., Nakazaki, N., Naruo, K., Okumura, S., Shimpo, S., Takeuchi, C., Wada, T., Watanabe, A., Yamada, M., Yasuda, M., and Taba, S. (1996) Sequence analysis of the genome of the unicellular Cyanobacterium *Synechocystis* sp. strain PCC6803. II. Sequence determination of the entire genome and assignment of potential protein-coding regions. *DNA Res. 3*, 109–136.

(2) Liu, X., Huang, W., and Wu, Q. (2006) Two-Component Signal Transduction Systems in the Cyanobacterium *Synechocystis* sp. PCC 6803. *Tsinghua Sci. Technol. 11*, 379–390.

(3) Hughes, J., Lamparter, T., Mittmann, F., Hartmann, E., Gärtner, W., Wilde, A., and Börner, T. (1997) A prokaryotic phytochrome. *Nature 386*, 663.

(4) Yeh, K. C., Wu, S. H., Murphy, J. T., and Lagarias, J. C. (1997) A cyanobacterial phytochrome two-component light sensory system. *Science 277*, 1505–1508.

(5) Aravind, L., and Ponting, C. P. (1997) The GAF domain: an evolutionary link between diverse phototransducing proteins. *Trends. Biochem. Sci. 22*, 458–459.

(6) Essen, L.-O., Mailliet, J., and Hughes, J. (2008) The structure of a complete phytochrome sensory module in the Pr ground state. *Proc. Natl. Acad. Sci. U.S.A. 105*, 14709–14714.

(7) Lagarias, J. C., and Rapoport, H. (1980) Chromopeptides from phytochrome. The structure and linkage of the Pr form of the phytochrome chromophore. *J. Am. Chem. Soc. 102*, 4821–4828.

(8) Lamparter, T., Esteban, B., and Hughes, J. (2001) Phytochrome Cph1 from the cyanobacterium *Synechocystis* PCC6803. Purification, assembly, and quaternary structure. *Eur. J. Biochem. 268*, 4720–4730.

(9) Wu, S. H., and Lagarias, J. C. (2000) Defining the bilin lyase domain: lessons from the extended phytochrome superfamily. *Biochemistry 39*, 13487–13495.

(10) Fry, K. T., and Mumford, F. E. (1971) Isolation and partial characterization of a chromophore-peptide fragment from pepsin digests of phytochrome. *Biochem. Biophys. Res. Commun. 45*, 1466–1473.

(11) Lamparter, T., Carrascal, M., Michael, N., Martinez, E., Rottwinkel, G., and Abian, J. (2004) The biliverdin chromophore binds covalently to a conserved cysteine residue in the N-terminus of *Agrobacterium* phytochrome Agp1. *Biochemistry 43*, 3659–3669.

(12) Kim, J. I., Shen, Y., Han, Y. J., Park, J. E., Kirchenbauer, D., Soh, M. S., Nagy, F., Schäfer, E., and Song, P. S. (2004) Phytochrome phosphorylation modulates light signaling by influencing the protein-protein interaction. *Plant Cell 16*, 2629–2640.

(13) Park, C. M., Shim, J. Y., Yang, S. S., Kang, J. G., Kim, J. I., Luka, Z., and Song, P. S. (2000) Chromophore-apoprotein interactions in *Synechocystis* sp. PCC6803 phytochrome cph1. *Biochemistry 39*, 6349–6356.

(14) Wagner, J. R., Brunzelle, J. S., Forest, K. T., and Vierstra, R. D. (2005) A light-sensing knot revealed by the structure of the chromophore-binding domain of phytochrome. *Nature 438*, 325–331.

(15) Furuya, M., and Song, P. S. (1994) Assembly and properties of holophytochrome in *Photomorphogenesis in Plants* (Kendrick, R. E., and Kronenberg, G. H. M., Eds.) 2nd ed., pp 105−140, Kluwer, Dordrecht.

(16) Song, C., Psakis, G., Lang, C., Mailliet, J., Gartner, W., Hughes, J., and Matysik, J. (2011) Two ground state isoforms and a chromophore D-ring photoflip triggering extensive intramolecular changes in a canonical phytochrome. *Proc. Natl. Acad. Sci. U. S. A. 108*, 3842–3847.

(17) Rüdiger, W., Thümmler, F., Cmiel, E., and Schneider, S. (1983) Chromophore structure of the physiologically active form Pfr of phytochrome. *Proc. Natl. Acad. Sci. U. S. A. 80*, 6244–6248.

(18) Inomata, K., Noack, S., Hammam, M. A., Khawn, H., Kinoshita, H., Murata, Y., Michael, N., Scheerer, P., Krauss, N., and Lamparter, T. (2006) Assembly of synthetic locked chromophores with *Agrobacterium* phytochromes Agp1 and Agp2. *J. Biol. Chem.* 28162–28173.

(19) Wagner, J. R., Zhang, J., Brunzelle, J. S., Vierstra, R. D., and Forest, K. T. (2007) High resolution structure of *deinococcus* bacteriophytochrome yields new insights into phytochrome architecture and evolution. *J. Biol. Chem. 282*, 12298–12309.

(20) Yang, X., Kuk, J., and Moffat, K. (2008) Crystal structure of *Pseudomonas aeruginosa* bacteriophytochrome: photoconversion and signal transduction. *Proc. Natl. Acad. Sci. U. S. A. 105*, 14715–14720.

(21) Yang, X., Kuk, J., and Moffat, K. (2009) Conformational differences between the Pfr and Pr states in *Pseudomonas aeruginosa* bacteriophytochrome. *Proc. Natl. Acad. Sci. U. S. A. 106*, 15639–15644.

(22) Scheerer, P., Michael, N., Park, J. H., Noack, S., Forster, C., Hammam, M. A., Inomata, K., Choe, H. W., Lamparter, T., and Krauss, N. (2006) Crystallization and preliminary X-ray crystallographic analysis of the N-terminal photosensory module of phytochrome Agp1, a biliverdin-binding photoreceptor from *Agrobacterium tumefaciens. J Struct. Biol. 153*, 97–102.

(23) Scheerer, P., Michael, N., Park, J. H., Nagano, S., Choe, H. W., Inomata, K., Borucki, B., Krauss, N., and Lamparter, T. (2010) Light-induced conformational changes of the chromophore and the protein in phytochromes: bacterial phytochromes as model systems. *ChemPhysChem 11*, 1090–1105.

(24) Rockwell, N. C., and Lagarias, J. C. (2006) The structure of phytochrome: a picture is worth a thousand spectra. *Plant Cell 18*, 4–14.

(25) Rockwell, N. C., and Lagarias, J. C. (2010) A brief history of phytochromes. *ChemPhysChem 11*, 1172–1180.

(26) Schneider-Poetsch, H. A. (1992) Signal transduction by phytochrome: phytochromes have a module related to the transmitter modules of bacterial sensor proteins. *Photochem. Photobiol. 56*, 839–846.

(27) Landgraf, F. T., Forreiter, C., Hurtado, P. A., Lamparter, T., and Hughes, J. (2001) Recombinant holophytochrome in *Escherichia coli*. *FEBS Lett. 508*, 459–462.

(28) Anders, K., von Stetten, D., Mailliet, J., Kiontke, S., Sineshchekov, V. A., Hildebrandt, P., Hughes, J. H., and Essen, L.-O. (2011) Spectroscopic and photochemical characterization of the red-light sensitive photosensory module of Cph2 from *Synechocystis* PCC 6803. *Photochem. Photobiol. 87*, 160–173.

(29) Lamparter, T., Mittmann, F., Gärtner, W., Börner, T., Hartmann, E., and Hughes, J. (1997) Characterization of recombinant phytochrome from the cyanobacterium *Synechocystis*. *Proc. Natl. Acad. Sci. U. S. A. 94*, 11792–11797.

(30) Hahn, J., Strauss, H. M., Landgraf, F. T., Gimenez, H. F., Lochnit, G., Schmieder, P., and Hughes, J. (2006) Probing protein-chromophore interactions in Cph1 phytochrome by mutagenesis. *FEBS J. 273*, 1415–1429.

(31) Bradford, M. (1976) A rapid and sensitive method for the quantitation of microgram quantities of protein utilizing the principles of protein-dye binding. *Anal. Biochem. 72*, 248–254.

(32) Quest, B., Hubschmann, T., Sharda, S., Tandeau de Marsac, N., and Gärtner, W. (2007) Homologous expression of a bacterial phytochrome. The cyanobacterium *Fremyella diplosiphon* incorporates biliverdin as a genuine, functional chromophore. *FEBS J. 274*, 2088–2098.

(33) Kyndt, J. A., Fitch, J. C., Seibeck, S., Borucki, B., Heyn, M. P., Meyer, T. E., and Cusanovich, M. A. (2010) Regulation of the Ppr histidine kinase by light-induced interactions between its photoactive yellow protein and bacteriophytochrome domains. *Biochemistry 49*, 1744–1754.

(34) Laemmli, U. K. (1970) Cleavage of structural proteins during the assembly of the head of bacteriophage T4. *Nature 227*, 680–685.

(35) Berkelman, T. R., and Lagarias, J. C. (1986) Visualization of bilin-linked peptides and proteins in polyacrylamide gels. *Anal. Biochem. 156*, 194–201.

(36) Pratt, L. H. (1975) Photochemistry of high molecular weight phytochrome in vitro. *Photochem. Photobiol. 22*, 33–36.

(37) Butler, W. L., Hendricks, S. B., and Siegelman, H. W. (1964) Action spectra of phytochrome in vitro. *Photochem. Photobiol. 3*, 521–528.

(38) Glazer, A. N., and Fang, S. (1973) Chromophore content of blue-green algal phycobiliproteins. *J. Biol. Chem. 248*, 659–662.

(39) Quest, B., Hubschmann, T., Sharda, S., Tandeau de Marsac, N., and Gärtner, W. (2007) Homologous expression of a bacterial phytochrome. The cyanobacterium *Fremyella diplosiphon* incorporates biliverdin as a genuine, functional chromophore. *FEBS J. 274*, 2088–2098.

(40) Strauss, H. M., Schmieder, P., and Hughes, J. (2005) Light-dependent dimerisation in the N-terminal sensory module of cyanobacterial phytochrome 1. *FEBS Lett. 18*, 3970–3974.

(41) Butler, W. L. (1972) in *Phytochrome* (Mitrakos, K., and Shropshire, W., Jr., Eds.) pp 185−192, Academic Press, New York.

(42) Wong, Y. S., McMichael, R. W. J. R., and Lagarias, J. C. (1989) Properties of a polycation-stimulated protein kinase associated with purified *Avena* phytochrome. *Plant Physiol. 91*, 709–718.

(43) Tasler, R., Moises, T., and Frankenberg-Dinkel, N. (2005) Biochemical and spectroscopic characterization of the bacterial phytochrome of *Pseudomonas aeruginosa*. *FEBS J. 272*, 1927–1936.

(44) Tasler, R., Moises, T., and Frankenberg-Dinkel, N. (2005) Biochemical and spectroscopic characterization of the bacterial phytochrome of *Pseudomonas aeruginosa*. *FEBS J. 272*, 1927–1936.

(45) Lamparter, T., Michael, N., Mittmann, F., and Esteban, B. (2002) Phytochrome from *Agrobacterium tumefaciens* has unusual spectral properties and reveals an N-terminal chromophore attachment site. *Proc. Natl. Acad. Sci. U. S. A. 99*, 11628–11633.

(46) Hübschmann, T., Jorissen, H. J., Börner, T., Gärtner, W., and Tandeau de Marsac, N. (2001) Phosphorylation of proteins in the light-dependent signalling pathway of a filamentous cyanobacterium. *Eur. J. Biochem. 268*, 3383–3389.

(47) Im, Y. J., Rho, S. H., Park, C. M., Yang, S. S., Kang, J. G., Lee, J. Y., Song, P. S., and Eom, S. H. (2002) Crystal structure of a cyanobacterial phytochrome response regulator. *Protein Sci. 11*, 614–624.

(48) Mukhopadhyay, D., Sen, U., Zapf, J., and Varughese, K. I. (2004) Metals in the sporulation phosphorelay: manganese binding by the response regulator Spo0F. *Acta Crystallogr., Sect. D: Biol. Crystallogr. 60*, 638–645.

(49) Kojetin, D. J., Thompson, R. J., Benson, L. M., Naylor, S., Waterman, J., Davies, K. G., Opperman, C. H., Stephenson, K., Hoch, J. A., and Cavanagh, J. (2005) Structural analysis of divalent metals binding to the *Bacillus subtilis* response regulator Spo0F: the possibility for *in vitro* metalloregulation in the initiation of sporulation. *Biometals 18*, 449–466.

(50) Grimshaw, C. E., Huang, S., Hanstein, C. G., Strauch, M. A., Burbulys, D., Wang, L., Hoch, J. A., and Whiteley, J. M. (1998) Synergistic kinetic interactions between components of the phosphorelay controlling sporulation in *Bacillus subtilis. Biochemistry 37*, 1365–1375.

(51) Bock, C. W., Katz, A. K., Markham, G. D., and Glusker, J. P. (1999) Manganese as a replacement for magnesium and zinc: Functional comparison of the divalent ions. *J. Am. Chem. Soc. 121*, 7360–7372.

(52) Hübschmann, T., Jorissen, H. J., Börner, T., Gärtner, W., and Tandeau de Marsac, N. (2001) Phosphorylation of proteins in the light-dependent signalling pathway of a filamentous cyanobacterium. *Eur. J. Biochem. 268*, 3383–3389.

(53) Stock, A. M., Robinson, V. L., and Goudreau, P. N. (2000) Two-component signal transduction, 69th ed., pp 183−215.

(54) Lukat, G. S., Lee, B. H., Mottonen, J. M., Stock, A. M., and Stock, J. B. (1991) Roles of the highly conserved aspartate and lysine residues in the response regulator of bacterial chemotaxis. *J. Biol. Chem. 266*, 8348–8354.

(55) Zapf, J., Madhusudan, M., Grimshaw, C. E., Hoch, J. A., Varughese, K. I., and Whiteley, J. M. (1998) A source of response regulator autophosphatase activity: the critical role of a residue adjacent to the Spo0F autophosphorylation active site. *Biochemistry 37*, 7725–7732.

(56) Huynh, T. N., Noriega, C. E., and Stewart, V. (2007) Conserved mechanism for sensor phosphatase control of two-component signaling revealed in the nitrate sensor NarX. *Proc. Natl. Acad. Sci. U. S. A. 107*, 21140–21145.

(57) Albanesi, D., Mansilla, M. C., and de Mendoza, D. (2004) The membrane fluidity sensor DesK of *Bacillus subtilis* controls the signal decay of its cognate response regulator. *J. Bacteriol. 186*, 2655–2663.

(58) Yoshida, T., Cai, S., and Inouye, M. (2002) Interaction of EnvZ, a sensory histidine kinase, with phosphorylated OmpR, the cognate response regulator. *Mol. Microbiol. 46*, 1283–1294.

(59) Möglich, A., Ayers, R. A., and Moffat, K. (2009) Design and signaling mechanism of light-regulated histidine kinases. *J. Mol. Biol. 385*, 1433–1444.

(60) Borthwick, H. A., Hendricks, S. B., Parker, M. W., Toole, E. H., and Toole, V. K. (1952) A Reversible Photoreaction Controlling Seed Germination. *Proc. Natl. Acad. Sci. U. S. A. 38*, 662–666.

(61) Möglich, A., and Moffat, K. (2007) Structural basis for light-dependent signaling in the dimeric LOV domain of the photosensor YtvA. *J. Mol. Biol.* *373*, 112–126.

(62) Levskaya, A., Chevalier, A. A., Tabor, J. J., Simpson, Z. B., Lavery, L. A., Levy, M., Davidson, E. A., Scouras, A., Ellington, A. D., Marcotte, E. M., and Voigt, C. A. (2005) Synthetic biology: engineering *Escherichia coli* to see light. *Nature* *438*, 441–442.